JOINT INSTITUTE FOR NUCLEAR RESEARCH
Frank Laboratory of Neutron Physics,
Department of Raman Spectroscopy

FINAL REPORT ON THE START PROGRAMME

Optical Characterization of Pristine and Er^{3+}/Yb^{3+}-Doped MoS_2 and UCNP Films Drop-Cast on MoS_2 and SiO_2 under 976 nm Excitation.

Supervisor:
Dr. Grigory M. Arzumanyan

Student:
Lilis Rachel Yohana, Indonesia
Universitas Gadjah Mada

Participation period:
September 14 – October 25,
Summer Session 2025

Dubna, 2025

1. Abstract

The Raman and photoluminescence (PL) spectroscopy were used to compare the characterization of chemical-vapor-deposited few-layer MoS_2 and its Er^{3+}/Yb^{3+}-co-doped analogue, as well as $NaGdF_4$:Er^{3+}/Yb^{3+} upconversion nanoparticles (UCNPs) that were chemically cast on MoS_2 and SiO_2 substrates. Er/Yb co-doping shows improved interlayer coupling and dopant-induced lattice disturbance by shifting the Raman modes ($E^1{}_{2g}$: 383.91 → 382.75 cm^{-1}; A_{1g}: 404.72 → 406.24 cm^{-1}) and increasing Δ from ≈20.8 to ≈23.5 cm^{-1} under 532 nm excitation. PL exhibits an A-exciton at 1.875 eV (661.48 nm). The intensity of A-exciton is significantly reduced by co-doping (~10×), which is consistent with the presence of additional nonradiative channels. Under 976 nm excitation, UCNPs exhibit detectable substrate-dependent modulation (quenching on MoS_2 vs SiO_2) and strong green/red upconversion (~525–545 nm, ~650 nm). These findings indicate that the lattice and excitonic properties of MoS_2 are effectively adjusted for optoelectronic and photonic applications through the use of rare-earth doping and UCNP coupling.

2. Introduction

2.1 CARS microspectrometer

Coherent Anti-Stokes Raman Scattering (CARS) represents a third-order nonlinear optical process involving the spatial and temporal overlap of two synchronized laser beams, specifically the pump beam at frequency $\omega_p$and the Stokes beam at frequency ω_s, on the sample. An anti-Stokes coherent signal at $\omega_{AS} = 2\omega_p - \omega_s$ is produced in the phase-matched (often forward) direction when the frequency difference $\Delta\omega = \omega_p - \omega_s$ coincides with a molecular vibrational mode. CARS imaging can be 10^2-10^4 times faster than spontaneous Raman under equivalent stimulation due to the molecular oscillators in-phase emission, which is extremely directed and amplified. Furthermore, because the released anti-Stokes photons are blue-shifted in relation to the excitation wavelengths, they fall outside of the usual fluorescence bands and are simple to separate using optical filters. In practice, CARS microscopy enables label-free vibrational imaging characterized by high sensitivity and an inherent capacity to reject fluorescent background (Li et al., 2020) (Malard et al., 2021).

The FLNP "Soliton" CARS microspectrometer is a multimodal 3D-scanning confocal platform that integrates spontaneous Raman, various CARS modes, and luminescence measurements. Its laser system consists of a picosecond $Nd:YVO_4$4 laser (Ekspla, PT257-SOPO, Lithuania) that provides a fixed 1064 nm Stokes beam and a tunable 690–990 nm pump beam, plus auxiliary lasers at 532, 633 and 785 nm for conventional Raman excitation. This design allows rapid switching between modalities: spontaneous Raman, forward/epi CARS (F-CARS/E-CARS), photoluminescence (PL), and even upconversion luminescence (UCL) detection. The microscope uses multiple PMTs and a CCD spectrometer for high-speed imaging and spectral registration. Importantly, near-IR excitation (including ~976 nm)

minimizes nonresonant background and photodamage while resonantly pumping Yb^{3+} ions in the doped UCNP films. Thus, this system can coherently probe MoS_2 vibrational modes (via CARS/Raman) and simultaneously capture Er^{3+}/Yb^{3+} upconversion emission under 976 nm pumping, making it ideally suited for studying pristine and doped MoS_2 and UCNP films on both MoS_2 and SiO_2 substrates.

Spontaneous Raman measurements are provided by dedicated continuous lasers at 532 nm (20 mW), 633 nm (15 mW) and 785 nm (100 mW) coupled into the confocal microscope. The Raman light that is collected is dispersed by an imaging monochromator (MS5004i) and recorded with a CCD (Proscan HS-101H). Additionally, high-speed detection is available through four PMT channels for multimodal mapping. For spontaneous Raman, spectrum registration spans approximately 50–6000 cm^{-1} with a spectral resolution of ≈0.9 cm^{-1} utilizing the 1200 gr/mm grating. A 60× (NA 1.2, water-immersion) objective provides spatial resolution of XY < 300 nm and Z ≈ 700 nm, which facilitates confocal Raman mapping of 2D materials. PL/UCL detection and the picosecond CARS laser system are fully integrated with these Raman capabilities to enable quick modal changeover.

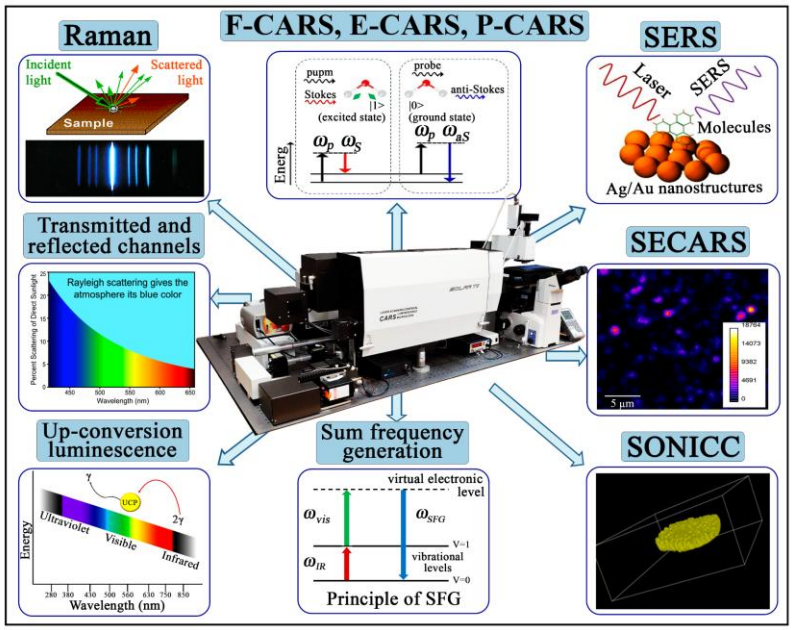

Figure 1. Microspectrometer "Confotec CARS" in Department of Raman Spectroscopy, FLNP JINR.

2.2 Sample Preparation

2.2.1 Pristine MoS_2

Pristine MoS_2 was synthesized via a chemical vapor deposition (CVD) method. Sulfur powder (45 mg) and molybdenum trioxide (MoO_3, 10.8 mg) were utilized as

precursor components. The growth was conducted in an atmosphere with regulated argon flow and pressure between 50 and 60 Pa. Initially, 50 sccm of argon gas was added. To ensure steady transport conditions during the sulfur sublimation process, the argon flow was first set to 45 sccm for a few minutes and then lowered to 35 sccm.

The precursor reaction was started by raising the substrate temperature to 675℃. Then, it was raised to 750℃, which was maintained for 8 minutes to enable the creation of MoS_2 layers. The system was naturally cooled to room temperature in an argon environment following the reaction.

2.2.2 Chemical casting of up conversion NPs on MoS_2 and Silicon dioxide (SiO_2)

The drop-casting method was used to deposit $NaGdF_4$ up-conversion nanoparticles (UCNPs) onto silicon dioxide (SiO_2) and MoS_2 substrates. A micropipette was used to create a colloidal dispersion of $NaGdF_4$ nanoparticles, which were then evenly deposited onto the target substrates surface. After that, the samples were allowed to dry at room temperature so that the solvent could naturally evaporate and create a thin layer of sticky nanoparticles.

This straightforward chemical casting method facilitates the integration of UCNPs with two-dimensional MoS_2 and dielectric SiO_2 substrates to facilitate advanced optical and spectroscopic characterization.

2.2.3 MoS_2 doped with Er^{3+}/Yb^{3+}

Chemical vapor deposition (CVD) was used for the fabrication of Er^{3+}/Yb^{3+}-doped MoS_2 films on SiO_2 substrates. The SiO_2 substrates were cleaned with an ultrasonic cleaner for five minutes each in ethanol, isopropanol (IPA), and deionized (DI) water before growth to get rid of organic and particle impurities.

For the precursor materials, the Mo and S sources were 10 mg of MoO_3 powder and 45 mg of sulfur, respectively. The rare-earth dopants were introduced with 5 mg of $ErCl_3$ and 5 mg of $YbCl_3$. The system was heated from ambient temperature to 150℃ during the synthesis, and argon was added at a pressure of 20 sccm. After that, the temperature was increased to 800℃ at a rate of 15℃ per minute while maintaining a pressure of 5 Pa and an argon flow of 100 sccm. The growth phase was sustained at 800℃ for 10 minutes under 50 sccm argon flow to ensure dopant inclusion into the MoS_2 lattice. Upon completion of growth, the system was organically cooled to room temperature.

2.3 Sample Characterization

2.3.1 Pristine MoS_2

Two main peaks are found in the Raman spectrum of pristine MoS_2 at 383.91 cm^{-1} and 404.72 cm^{-1}. These peaks correspond to the $E^1{}_{2g}$ (in-plane) and A_{1g} (out-of-plane) vibrational modes, respectively (Liu et al., 2021). These frequencies nearly match reported values for monolayer MoS_2 ($E^1{}_{2g}$ ≈384-386 cm^{-1}, A_{1g} ≈404-405 cm^{-1}) (Wu et al., 2013). The mode separation $\Delta\omega$, which is approximately 20.8 cm^{-1}, is also within the average monolayer range of approximately 19–21 cm^{-1} (Wu et al., 2013). In contrast, bulk MoS_2 displays $E^1{}_{2g}$ at approximately 382 cm^{-1} and A_{1g} at around 408 cm^{-1}, resulting in a frequency difference of approximately 26 cm^{-1} (Van Velson et al., 2023). As a result, our Raman shifts and $\Delta\omega$ measurements are consistent with an atomically thin film (monolayer or few-layer), as the thickness increases, causing $E^1{}_{2g}$ to redshift and A_{1g} to blueshift, thereby increasing their separation (Wu et al., 2013) (Van Velson et al., 2023).

The FWHM values for the Raman peaks of pristine MoS_2 at 383.91 cm^{-1} ($E^1{}_{2g}$) and 404.72 cm^{-1} (A_{1g}) are 5.63 cm^{-1} and 6.43 cm^{-1}, respectively. The FWHM values for $E^1{}_{2g}$ and A_{1g} are typically 3–4 cm^{-1} and 4–5 cm^{-1}, respectively, which are marginally broader than those reported for high-quality monolayer MoS_2. One example is the work of (Yu et al., 2013) who found that in exfoliated monolayers, the $E^1{}_{2g}$ and A_{1g} linewidths were around 3.7 cm^{-1} and 4.2 cm^{-1}, respectively. The narrow peaks below 5 cm^{-1} for few-layer MoS_2 were also observed by (Lee et al., 2010).

The FWHM values in this measurement are marginally larger, which suggests that there is mild structural disorder, multilayer formation, or substrate-induced effects. Raman peaks can be broadened by elements like strain, surface roughness, or charge impurities on SiO_2/Si substrates, particularly the A_{1g} mode, which is susceptible to out-of-plane interactions. In general, the linewidths that were obtained are within the acceptable range for MoS_2 that is either CVD-grown or substrate-supported, suggesting that the crystalline quality is reasonably good, despite minimal inhomogeneity.

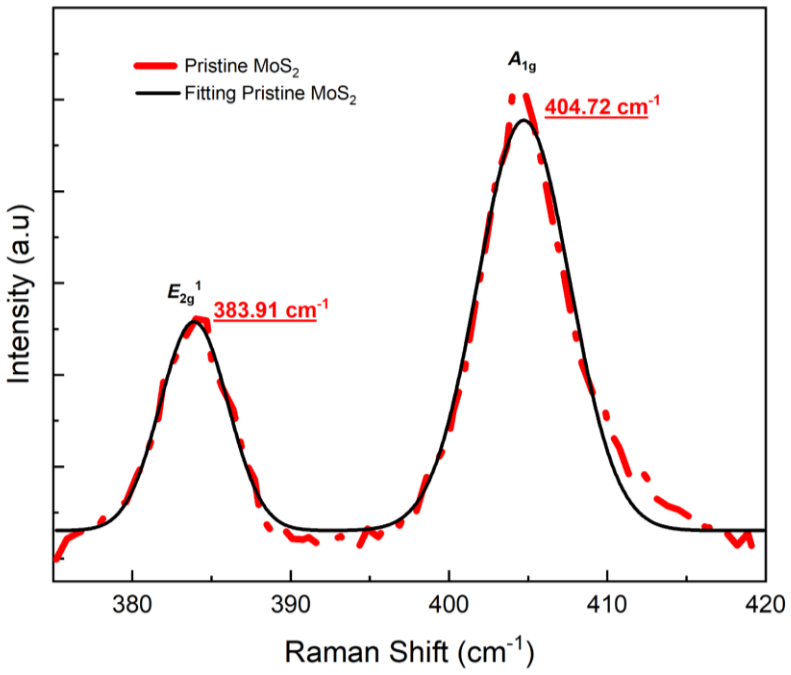

Figure 2. Raman spectrum of pristine MoS_2

Photoluminescence (PL) offers additional evidence of monolayer structure. Bulk MoS_2 functions as an indirect-gap semiconductor, exhibiting a bandgap of approximately 1.2–1.3 eV and minimal photoluminescence at room temperature (Splendiani et al., 2010). In contrast, monolayer MoS_2 possesses a direct bandgap of around 1.8–1.9 eV at the K-point (Liu et al., 2021). The PL peak in our sample at 665.02 nm (1.865 eV) is exactly the same as the monolayer MoS_2 A-exciton emission. The direct-band-gap monolayer is distinguished by the presence of this robust PL peak; alternatively, it would be absent or significantly diminished in bulk or multilayer materials (Splendiani et al., 2010). The measured 1.865 eV emission shows that tightly bound neutral excitons are recombining in the direct gap. In conclusion, the significant PL at 1.865 eV and the Raman mode positions (and their ~20.8 cm^{-1} splitting) are entirely consistent with pure monolayer (or very few-layer) MoS_2, demonstrating its strong excitonic direct-gap emission and two-dimensional lattice vibrations (Wu et al., 2013) (Splendiani et al., 2010).

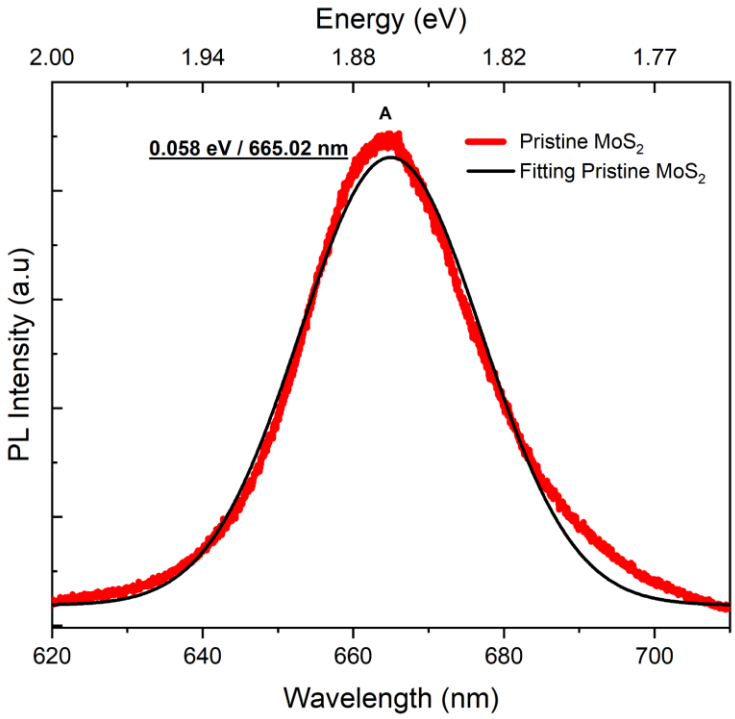

Figure 3. PL spectrum of pristine MoS_2

2.3.2 Chemical casting of up-conversion NPs on MoS_2 and Silicon dioxide (SiO_2)

Under 976 nm excitation, the $NaGdF_4$-based UCNPs exhibit intense visible upconversion luminescence, whereas MoS_2 alone exhibits virtually no emission. Strong green and red bands (approximately 525–545 nm and ~650 nm, respectively) are observed in both the UCNP_SiO_2 and UCNP_MoS_2 samples, which are indicative of lanthanide upconversion transitions (Ji et al., 2020). These correspond to well-known f-f emissions (for example, Er^{3+}: $^2H_{11/2}/\ ^4S_{3/2} \rightarrow\ ^4I_{15/2}$ at ~525/545 nm and $^4F_{19/2} \rightarrow\ ^4I_{15/2}$ at ~650 nm (Ji et al., 2020)) or equivalent transitions in other dopants. Pristine MoS_2, on the other hand, produces very little light in these circumstances because it does not efficiently absorb 976 nm (its band gap is approximately 1.2–1.9 eV). Since SiO_2 is transparent and optically inert, the UCNP_SiO_2 hybrid quantitatively replicates the inherent brightness of the $NaGdF_4$ UCNPs, whereas the emission intensity of the UCNP_MoS_2 hybrid represents both the UCNP emission and any interfacial effects.

The substrate is crucial in influencing the emission of UCNP. The observed spectra are basically those of the particles themselves because silicon dioxide is an optically transparent and chemically inert host that neither absorbs nor quenches the UCNP emission. On the other hand, 2D MoS_2 can interact significantly with emitters that are close by. The energy transfer from the excited UCNPs to the MoS_2 in the UCNP_MoS_2 system has the potential to open nonradiative decay channels. Indeed, MoS_2 is widely recognized as an effective fluorescence quencher (Choi et al., 2021), with some even describing it as

having "extreme" quenching capabilities for nearby fluorophores (Yuan et al., 2020). Therefore, if the emission from UCNP_MoS_2 is less than that from UCNP–SiO_2, it can be explained by either charge transfer into MoS_2 or Förster-type resonance energy transfer. In contrast, any unexpected improvement would suggest a photonic coupling effect. For instance, the high dielectric constant and excitonic resonances of MoS_2 could potentially increase radiative rates by modifying the local photonic density of states or near-field, similar to the reported plasmonic or superlens enhancements of UCL (Ji et al., 2020). However, in practice, pristine MoS_2 most frequently quenches rather than amplifies UCNP emission. In conclusion, the green/red UCL bands in UCNP_MoS_2 and UCNP_SiO_2 both originate from the doped $NaGdF_4$ nanoparticles. However, SiO_2 merely supports the particles (no spectral change), whereas MoS_2 introduces interfacial interactions (notably quenching via energy transfer) that can reduce or modify the upconversion intensity (Choi et al., 2021) (Yuan et al., 2020).

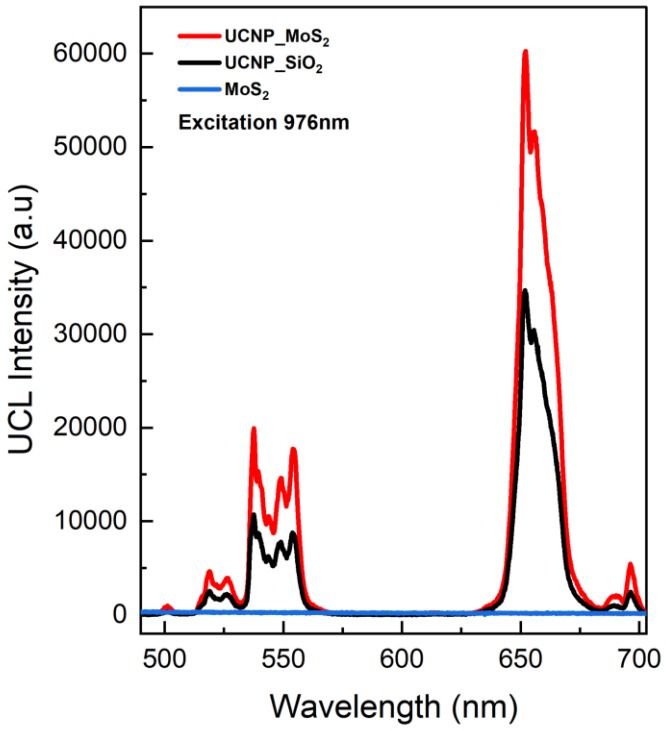

Figure 4. Upconversion luminescence spectrum of UCNP on MoS_2, UCNP on SiO_2, and pristine MoS_2

2.3.3 MoS_2 doped with Er^{3+}/Yb^{3+}

In pristine MoS_2, the two Raman-active modes are observed at values characteristic of few-layer films: the in-plane $E^1{}_{2g}$ mode at approximately 384 cm^{-1} and the out-of-plane A_{1g} mode at approximately 405 cm^{-1}. Monolayer MoS_2 exhibits peaks at

approximately 385 and 404 cm^{-1} (Δ approximately 19 cm^{-1}) (Soni et al., 2023), whereas bilayer MoS_2 displays peaks at approximately 390 and 410 cm^{-1} (Δ approximately 20.5 cm^{-1}) (Gaur et al., 2019). ${E^1}_{2g}$≈383.9 cm^{-1} and A_{1g}≈404.7 cm^{-1} (Δ≈20.8 cm^{-1}) in our measurements for the undoped MoS_2 are consistent with a few-layer thickness (≈2–3 layers) (Soni et al., 2023) (Heng et al., 2023). By co-doping Er^{3+}/Yb^{3+}, ${E^1}_{2g}$ decreases to approximately 382.8 cm^{-1}, while A_{1g} increases to approximately 406.2 cm^{-1}. Consequently, Δ increases to approximately 23.5 cm^{-1}. This difference is significant in comparison to undoped MoS_2, as an increase in Δ often signifies the presence of more layers or stronger interlayer coupling (Heng et al., 2023). Electron-doping usually softens A_{1g} (Ge and Liu, 2013), but the observed ${E^1}_{2g}$ softening (red-shift) and A_{1g} hardening (blue-shift) post doping are the contrary. Indeed, a blue-shift of A_{1g} is a characteristic of compressive strain or p-type doping (Nan et al., 2014) (Yan et al., 2012). A_{1g} is also known to be elevated (blue-shifted) by compressive strain (Yan et al., 2012), while it is red-shifted by tensile strain. Therefore, the sum of the effects indicates that the incorporation of Er/Yb results in either hole-doping or a lattice compression. The larger Δ (approximately 23–24 cm^{-1}) is comparable to the values reported for multilayer or strained MoS_2 (Heng et al., 2023). In conclusion, the Raman modes are shifted by Er/Yb co-doping in a manner that is consistent with the addition of interlayer interaction and p-type (or compressive) perturbation. Specifically, A_{1g} is up-shifted by approximately 1.5 cm^{-1}, while ${E^1}_{2g}$ is down-shifted by approximately 1.2 cm^{-1} relative to pristine. This trend is consistent with previous reports that p-type dopants induce an A_{1g} blue-shift (${E^1}_{2g}$ remains relatively unaltered) (Nan et al., 2014), whereas unintentional n-doping or lattice expansion would have the opposite effect (Ge and Liu, 2013) (Yan et al., 2012).

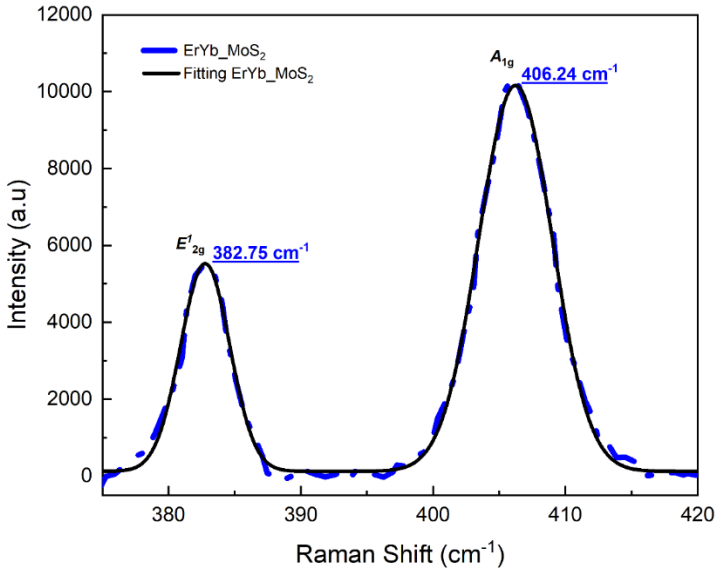

Figure 5. Raman spectrum of MoS_2 doped with Er^{3+}/Yb^{3+}

Upon co-doping, the maximal separation $\Delta=A_{1g}–E^1{}_{2g}$ increases from approximately 20.8 to 23.5 cm^{-1}. In contrast, bulk MoS_2 can reach ≈25 cm^{-1}, while monolayer MoS_2 has $\Delta\approx19$ cm^{-1} (Soni et al., 2023). As a result, the doped film's Δ is in the few-layer regime, while our pristine film behaves like approximately 2–3 layers. In general, Δ increases with the number of layers or strain (Heng et al., 2023). The doping-induced increase in Δ is consistent with the A_{1g} blue-shift noted above, suggesting enhanced interlayer coupling or a small compressive strain. Bilayers have Δ~20–21 cm^{-1}, monolayer MoS_2 has Δ~19 cm^{-1} (Soni et al., 2023), and heavily-strained or doped films can reach the mid-20s (Heng et al., 2023) (Yan et al., 2012). These findings are consistent with prior investigations. In summary, the MoS_2 is induced to exhibit a thicker or strained Raman signature as a result of Er/Yb co-doping.

The photoluminescence of Er/Yb_ MoS_2 exhibits one distinct excitonic peaks. The peak is located at approximately 1.875 eV (661.5 nm. These correspond to the A-excitons of MoS_2, respectively. In the literature, the A-exciton is typically located in the range of 1.85–1.90 eV (approximately 660–670 nm) (Soni et al., 2023). Indeed, A-excitons in monolayer MoS_2 are assigned 1.88 eV (Soni et al., 2023), respectively, by steady-state absorption/PL investigations. These numbers are exactly where our measured peak energies fall, indicating that Peak 1 is the emission of the A-exciton.

In contrast to undoped MoS_2, the PL of the co-doped film is significantly quenched. Compared to pristine MoS_2 under the same excitation, the A-exciton peak of Er/Yb: MoS_2 in our data is about an order of magnitude weaker. This significant decrease in the quantum yield of PL is in accordance with prior reports that have indicated the introduction of nonradiative channels by added dopants or carriers. For example, the A-exciton optical peaks have been demonstrated to be quenched by chemical or charge doping of MoS_2, resulting in the conversion of neutral excitons into less-radiative trions or charged excitons (Dhakal et al., 2014) (Nan et al., 2014). While severe doping usually reduces overall PL, in one study a p-type adsorbate (O_2) boosted the PL by converting trions into excitons (Nan et al., 2014). In our experiment, Er/Yb ions most likely transfer charge and produce defect states, which lower exciton recombination.

Additionally, we observe a minor blue-shift of the A-exciton: the fitted peak shifts from approximately 665.0 nm (1.864 eV, undoped) to 661.5 nm (1.875 eV) in the doped film. This approximately 10 meV shift to higher energy indicates a potential p-type or strain effect. Similarly, the MoS_2 PL has been shown to blueshift from trion (X^-) to neutral-exciton (X) emission when adsorbed oxygen (a p-dopant) is present (Nan et al., 2014). The bandgap may be similarly stiffened in this case by the narrowing of surplus electrons (via Er/Yb interactions). The inhomogeneous broadening from disorder is suggested by the fact that the maximal linewidth (several tens of meV) remains broad.

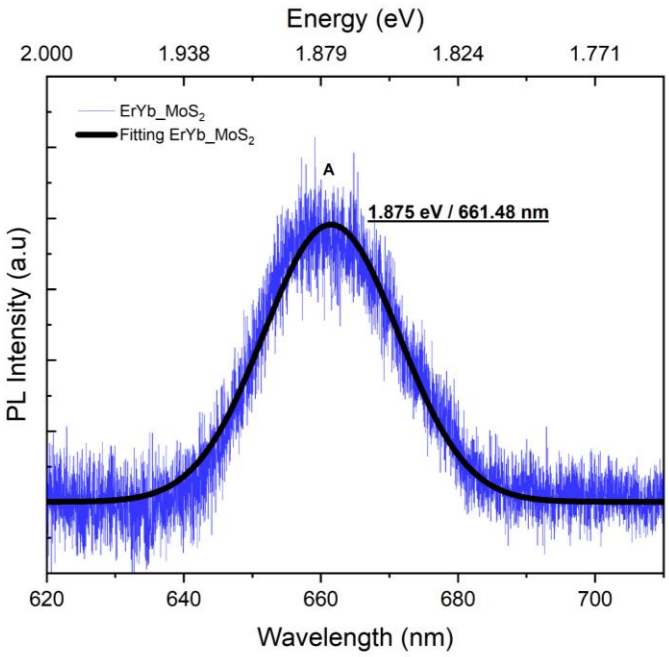

Figure 6. PL spectrum of MoS_2 doped with Er^{3+}/Yb^{3+} on the region 661.48 nm

In conclusion, the interpeak spacing Δ is increased by the Er^{3+}/Yb^{3+} co-doping of MoS_2, which hardens A_{1g} and boarders $E^1{}_{2g}$. In contrast to basic electron doping, this suggests p-type character or lattice compression. The behavior of thicker or stretched MoS_2 is reflected in the increased Δ and mode shifts. The excitonic peaks in PL correspond to the known A (∼1.88 eV) and B (∼2.04 eV) transitions, and the emission at 607 nm is due to the B-exciton instead of any Er^{3+}/Yb^{3+} line. The intensity of the PL is significantly reduced by Er/Yb doping, which is likely due to nonradiative defects or carrier transfer. Additionally, the A-exciton undergoes a slight blue shift. This observation is consistent with previous research on rare-earth optical transitions and doped/strained MoS_2, which supports our mode assignments and interpretations.

3. Results

Two main MoS_2 modes demonstrate opposite shifts in the films that are pristine and those that have been doped with Er^{3+}/Yb^{3+}. Specifically, the in-plane $E^1{}_{2g}$ mode red undergoes a shift from 383.91 to 382.75 cm^{-1} (~ –1.16 cm^{-1}), whereas the out-of-plane A_{1g} mode blue undergoes a shift from 404.72 to 406.24 cm^{-1} (~ +1.52 cm^{-1}). In monolayer MoS_2, compressive strain increases A_{1g}, while tensile strain decreases both modes (with $E^1{}_{2g}$ shifting a greater amount). A complex strain/doping state is suggested by the observed pattern ($E^1{}_{2g}$ down, A_{1g} up), which is likely a local compressive distortion from RE incorporation (hardening A_{1g}) coexisting with in-plane expansion (softening $E^1{}_{2g}$). In contrast, strain or lattice distortion appears to be dominating in this case, as simple electron doping usually red-shifts A_{1g} (Yan et al., 2012). In the doped film,

the mode separation Δ ($= \omega_{A_{1g}} - \omega_{E^1{}_{2g}}$) increases significantly, from about 20.8 to around 23.5 cm^{-1}. A pristine monolayer has a thickness of approximately 19 cm^{-1} (Lyu et al., 2019), while few-layer or bulk MoS_2 have a thickness of approximately 25 cm^{-1}. Thus, the increased Δ implies that the rare-earth dopants have induced lattice stiffening or enhanced interlayer coupling. In summary, the shifts and increased Δ suggest that the incorporation of Er^{3+}/Yb^{3+} has resulted in substantial strain and structural perturbation, rather than pure charge doping (Lyu et al., 2019).

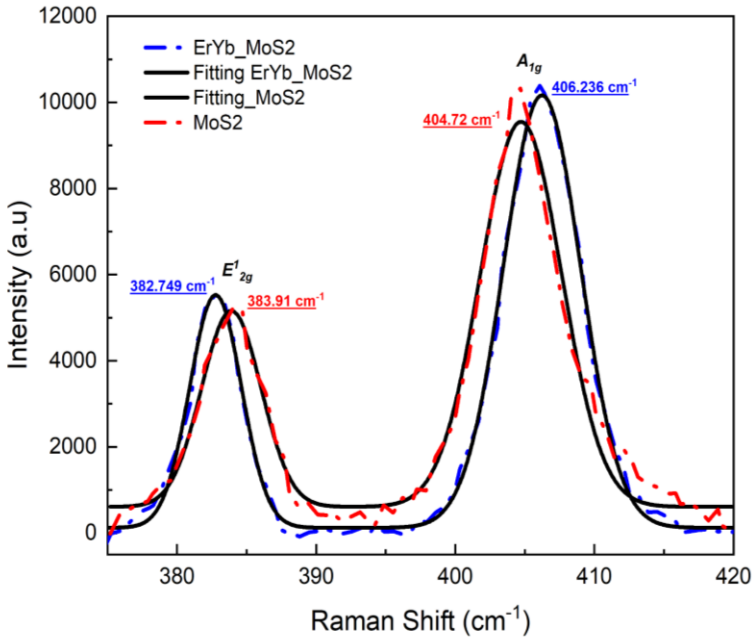

Figure 7. Raman spectrum of pristine MoS_2 and MoS_2 doped with Er^{3+}/Yb^{3+}.

A minor shift in the A-exciton peak of MoS_2 is also observed as a result of doping. The A exciton is visible at 1.864 eV (665.0 nm) in the pristine film and at 1.874 eV (661.5 nm) in the Er^{3+}/Yb^{3+}-doped film, which represents a blueshift of about 10 meV. This minor increase in energy may be indicative of a slight enlargement of the bandgap or modified screening as a result of dopant-induced strain or dielectric changes. On the other hand, a previous investigation discovered that Er-doping resulted in a modest red-shift of the A peak (Lyu et al., 2019). Consequently, the blue shift observed in this study is likely indicative of a distinct strain/electric-field environment. It is worth noting that the doped sample possesses an additional peak at 607.36 nm (2.0416 eV) that is not present in the pristine film. This energy is in near agreement with the MoS_2 B-exciton (approximately 2.04 eV) that has been observed in the literature (Soni et al., 2025). There are no known Er^{3+} or Yb^{3+} f–f transitions that occur near 2.04 eV (Soni et al., 2025). However, numerous investigations have reported the B exciton of monolayer MoS_2 around 2.04 eV. The 607 nm characteristic is most likely caused by the MoS_2 B exciton, which may be affected by impurity levels, rather than rare-earth emission. To conclude, the PL alterations, which consist of a slight blue-shift of the A peak and the emergence of the B exciton emission, are

consistent with lattice modification induced by RE, rather than the formation of new RE luminescence centers (Lyu et al., 2019) (Soni et al., 2025).

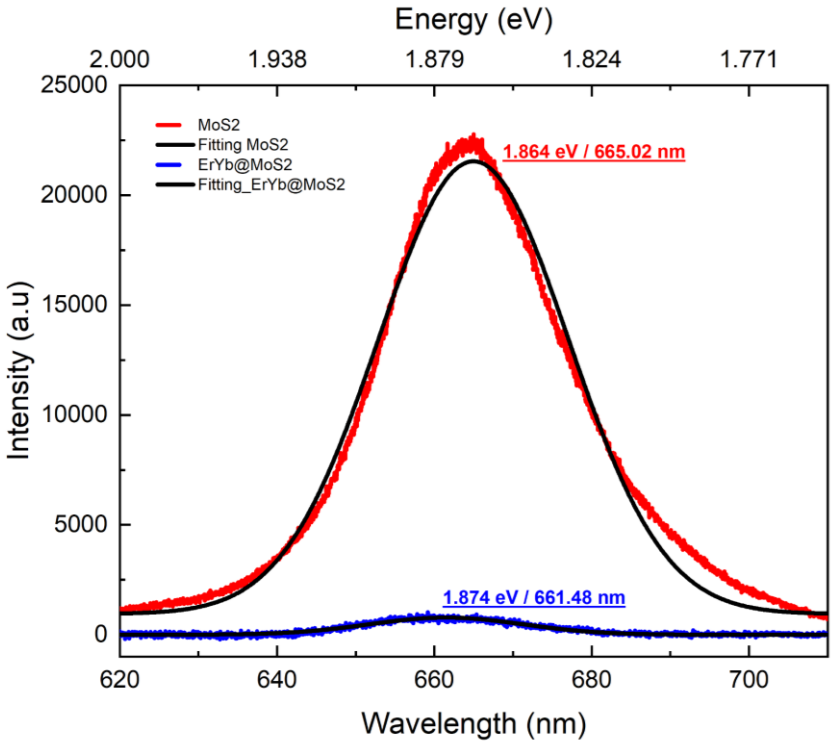

Figure 8. PL spectrum of pristine MoS_2 and MoS_2 doped with Er^{3+}/Yb^{3+}.

4. Conclusion

Raman and steady-state PL (532 nm excitation, room temperature) were employed to characterize CVD-grown, few-layer MoS_2 and its Er^{3+}/Yb^{3+} co-doped counterpart. The primary conclusions included:

a. Raman signatures indicate dopant-induced lattice perturbation.

Er^{3+}/Yb^{3+} co-doping results in an $E^1{}_{2g}$ down-shift from 383.91 → 382.75 cm^{-1} (≈–1.16 cm^{-1}) and an A_{1g} up-shift from 404.72 → 406.24 cm^{-1} (≈+1.52 cm^{-1}), thereby increasing the intermode separation Δ from 20.8 cm^{-1} to 23.5 cm^{-1}. Local lattice distortion (strain) and strengthened interlayer coupling (or effective "thickening") induced by substitutional rare-earth incorporation, rather than straightforward n-type electron doping, are the most consistent explanations for these opposite-direction shifts and larger Δ.

b. PL shows reduced quantum yield.

On doping, the A-exciton is slightly blue-shifted and remains observable (1.864 → 1.875 eV; 665.02 → 661.48 nm, ≈+10 meV), which is consistent with the modified dielectric screening/strain.

c. Doping trade-offs, exciton visibility vs. PL quenching.

Overall A-exciton PL intensity is significantly quenched (approximately one order of magnitude lower than pristine under identical conditions). This indicates that, although dopant-induced modifications can increase the radiativity of specific excitonic channels (or reduce their masking by competing channels), co-doping also introduces non-radiative traps and charge-transfer pathways that decrease the net quantum yield, which is consistent with previous reports on doped/defective MoS_2.

In summary, the excitonic character of MoS_2 (A excitons) is maintained by Er^{3+}/Yb^{3+} co-doping, which also induces lattice strain and stronger interlayer coupling, which alter and reshape vibrational and optical responses.

5. Acknowledgements

I would like to express my deepest gratitude to Dr. Grigory Arzumanyan for his guidance, patience, and constant support throughout my Summer Student Program. His guidance not only helped me comprehend the subject in depth, but it also motivated me to advance as a researcher.

My heartfelt gratitude also goes to Le Duc Huy, Kahramon Z. Mamatkulov, Yersultan Arynbek, Khlood A. A. Abdeljawaad, Pham Ngoc Bao Tri, and all members of the team for their wonderful assistance, talks, and support throughout this endeavor. Their guidance and collaboration contributed to a meaningful and pleasurable experience.

I am grateful for the laboratory's welcoming and motivating environment, which made every day of work a worthwhile learning experience. Finally, I'd like to thank the Joint Institute for Nuclear Research (JINR) for providing me with the opportunity to participate in real-world scientific research, as well as for their financial and organizational assistance, which enabled this internship.

References

Choi, J. W., Yoon, J., Lim, J., Shin, M., & Lee, S. N. (2021). Graphene/MoS2 nanohybrid for biosensors. *Materials*, *14*(3), 1–22.

Dhakal, K. P., Duong, D. L., Lee, J., Nam, H., Kim, M., Kan, M., Lee, Y. H., & Kim, J. (2014). Confocal absorption spectral imaging of MoS2: Optical transitions depending on the atomic thickness of intrinsic and chemically doped MoS2. *Nanoscale*, *6*(21), 13028–13035.

Gaur, A., Chiappe, D., Lin, D., Cott, D., Asselberghs, I., Heyns, M., & Radu, I. (2019). Analysis of admittance measurements of MOS capacitors on CVD grown bilayer MoS2. *2D Materials*, *6*(3).

Ge, Y., & Liu, A. Y. (2013). Phonon-mediated superconductivity in electron-doped single-layer MoS 2: A first-principles prediction. *Physical Review B - Condensed Matter and Materials Physics*, *87*(24).

Heng, C., Wang, X., Zhao, C., Wu, G., Lv, Y., Wu, H., Zhao, M., & Finstad, T. G. (2023). Ultrathin Rare-Earth-Doped MoS2 Crystalline Films Prepared with Magnetron Sputtering and Ar + H2 Post-Annealing. *Crystals*, *13*(2).

Ji, Y., Xu, W., Ding, N., Yang, H., Song, H., Liu, Q., Ågren, H., Widengren, J., & Liu, H.

(2020). Huge upconversion luminescence enhancement by a cascade optical field modulation strategy facilitating selective multispectral narrow-band near-infrared photodetection. *Light: Science and Applications*, *9*(1).

Lee, C., Yan, H., Brus, L. E., Heinz, T. F., Hone, J., & Ryu, S. (2010). Anomalous lattice vibrations of single- and few-layer MoS2. *ACS Nano*, *4*(5), 2695–2700.

Li, S., Li, Y., Yi, R., Liu, L., & Qu, J. (2020). Coherent Anti-Stokes Raman Scattering Microscopy and Its Applications. *Frontiers in Physics*, *8*(December), 1–9.

Liu, X., Yi, J., Yang, S., Lin, E. C., Zhang, Y. J., Zhang, P., Li, J. F., Wang, Y., Lee, Y. H., Tian, Z. Q., & Zhang, X. (2021). Nonlinear valley phonon scattering under the strong coupling regime. *Nature Materials*, *20*(9), 1210–1215.

Lyu, Y., Wu, Z., Io, W. F., & Hao, J. (2019). Observation and theoretical analysis of near-infrared luminescence from CVD grown lanthanide Er doped monolayer MoS2 triangles. *Applied Physics Letters*, *115*(15).

Malard, L. M., Lafeta, L., Cunha, R. S., Nadas, R., Gadelha, A., Cançado, L. G., & Jorio, A. (2021). Studying 2D materials with advanced Raman spectroscopy: CARS, SRS and TERS. *Physical Chemistry Chemical Physics*, *23*(41), 23428–23444.

Nan, H., Wang, Z., Wang, W., Liang, Z., Lu, Y., Chen, Q., He, D., Tan, P., Miao, F., Wang, X., Wang, J., & Ni, Z. (2014). Strong photoluminescence enhancement of MoS2 through defect engineering and oxygen bonding. *ACS Nano*, *8*(6), 5738–5745.

Soni, A., Kamath, N. S., Shen, Y. Y., Seksaria, H., De Sarkar, A., Chang, W. H., & Pal, S. K. (2025). Substrate-induced modulation of transient optical response of large-area monolayer MoS2. *Scientific Reports*, *15*(1), 1–16.

Soni, A., Kushavah, D., Lu, L. S., Chang, W. H., & Pal, S. K. (2023). Efficient Multiple Exciton Generation in Monolayer MoS2. *Journal of Physical Chemistry Letters*, *14*(12), 2965–2972.

Splendiani, A., Sun, L., Zhang, Y., Li, T., Kim, J., Chim, C. Y., Galli, G., & Wang, F. (2010). Emerging photoluminescence in monolayer MoS2. *Nano Letters*, *10*(4), 1271–1275.

Van Velson, N., Zobeiri, H., & Wang, X. (2023). Thickness-Dependent Raman Scattering from Thin-Film Systems. *Journal of Physical Chemistry C*, *127*(6), 2995–3004.

Wu, S., Huang, C., Aivazian, G., Ross, J. S., Cobden, D. H., & Xu, X. (2013). Vapor-solid growth of high optical quality MoS2 monolayers with near-unity valley polarization. *ACS Nano*, *7*(3), 2768–2772.

Yan, R., Bertolazzi, S., Brivio, J., Fang, T., Konar, A., Birdwell, A. G., Nguyen, N. V., Kis, A., Jena, D., & Xing, H. G. (2012). *Raman and Photoluminescence Study of Dielectric and Thermal Effects on Atomically Thin MoS2*. 1–17.

Yu, Y., Li, C., Liu, Y., Su, L., Zhang, Y., & Cao, L. (2013). Controlled scalable synthesis of uniform, high-quality monolayer and few-layer MoS2 films. *Scientific Reports*, *3*, 1–6.

Yuan, Y., Yu, H., & Yin, Y. (2020). A highly sensitive aptasensor for vascular endothelial growth factor based on fluorescence resonance energy transfer from upconversion nanoparticles to MoS2nanosheets. *Analytical Methods*, *12*(36), 4466–4472.